

PD1 inhibits PKC θ -dependent phosphorylation of cytoskeleton-related proteins and immune synapse formation

Daniela Chmiest,¹ Silvia Podavini,¹ Kalliopi Ioannidou,² David Vallois,² Chantal Décaillet,¹ Montserrat Gonzalez,¹ Manfredo Quadroni,³ Kevin Blackney,⁴ Rebekka Schairer,⁵ Laurence de Leval,² and Margot Thome¹

¹Department of Immunobiology, University of Lausanne, Epalinges, Switzerland; ²Department of Laboratory Medicine and Pathology, Institute of Pathology, Lausanne University Hospital and University of Lausanne, Lausanne, Switzerland; ³Protein Analysis Facility, University of Lausanne, Lausanne, Switzerland; ⁴Flow Cytometry Facility, Department of Formation and Research, University of Lausanne, Epalinges, Switzerland; and ⁵Department of Internal Medicine II, Hematology, Oncology, Clinical Immunology, and Rheumatology, University Hospital Tübingen, Tübingen, Germany

Key Points

- PD1 inhibits PKC θ synaptic localization and phosphorylation of its cytoskeleton targets, leading to formation of smaller immune synapses.
- Reduced Vimentin phosphorylation on S39 is a putative marker for PD1 engagement in T cells in a PDL1⁺ tumor microenvironment.

The inhibitory surface receptor programmed cell death protein 1 (PD1) is a major target for antibody-based cancer immunotherapies. Nevertheless, a substantial number of patients fail to respond to the treatment or experience adverse effects. An improved understanding of intracellular pathways targeted by PD1 is thus needed to develop better predictive and prognostic biomarkers. Here, via unbiased phosphoproteome analysis of primary human T cells, we demonstrate that PD1 triggering inhibited the phosphorylation and physical association with protein kinase C θ (PKC θ) of a variety of cytoskeleton-related proteins. PD1 blocked activation and recruitment of PKC θ to the forming immune synapse (IS) in a Src homology-2 domain-containing phosphatase-1/2 (SHP1/SHP2)-dependent manner. Consequently, PD1 engagement led to impaired synaptic phosphorylation of cytoskeleton-related proteins and formation of smaller IS. T-cell receptor induced phosphorylation of the PKC θ substrate and binding partner vimentin was long-lasting and it could be durably inhibited by PD1 triggering. Vimentin phosphorylation in intratumoral T cells also inversely correlated with the levels of the PD1 ligand, PDL1, in human lung carcinoma. Thus, PKC θ and its substrate vimentin represent important targets of PD1-mediated T-cell inhibition, and low levels of vimentin phosphorylation may serve as a biomarker for the activation of the PD1 pathway.

Introduction

T cells are crucial for effective anticancer immune responses. Their activation requires triggering of the T-cell receptor (TCR) by major histocompatibility complex (MHC)-bound antigen, together with a costimulatory signal provided by the CD28 coreceptor.^{1,2} This initiates a complex signaling cascade that involves the membrane-proximal tyrosine kinases Lck and ZAP70 and the serine/threonine (S/T) kinase PKC θ (protein kinase C θ), and culminates in the induction of major transcriptional changes.¹⁻³ Upon activation, the T cell and the antigen-presenting cells also form a stable, mature immune synapse (IS), required for polarized secretion of inflammatory cytokines and restricted killing of target cells.⁴⁻⁶

Submitted 10 October 2023; accepted 20 February 2024; prepublished online on *Blood Advances* First Edition 21 March 2024. <https://doi.org/10.1182/bloodadvances.2023011901>.

The mass spectrometry proteomics data have been deposited to the ProteomeXchange Consortium via the PRIDE partner repository with the data set identifier PXD044028.

Data may be accessed at <http://www.ebi.ac.uk/pride> (username: reviewer_pxd044028@ebi.ac.uk, password: paxjQmcF).

The other original data that support the findings of this study are available on reasonable request from the corresponding author, Margot Thome (margot.thomemiazza@unil.ch).

The full-text version of this article contains a data supplement.

© 2024 by The American Society of Hematology. Licensed under [Creative Commons Attribution-NonCommercial-NoDerivatives 4.0 International \(CC BY-NC-ND 4.0\)](https://creativecommons.org/licenses/by-nc-nd/4.0/), permitting only noncommercial, nonderivative use with attribution. All other rights reserved.

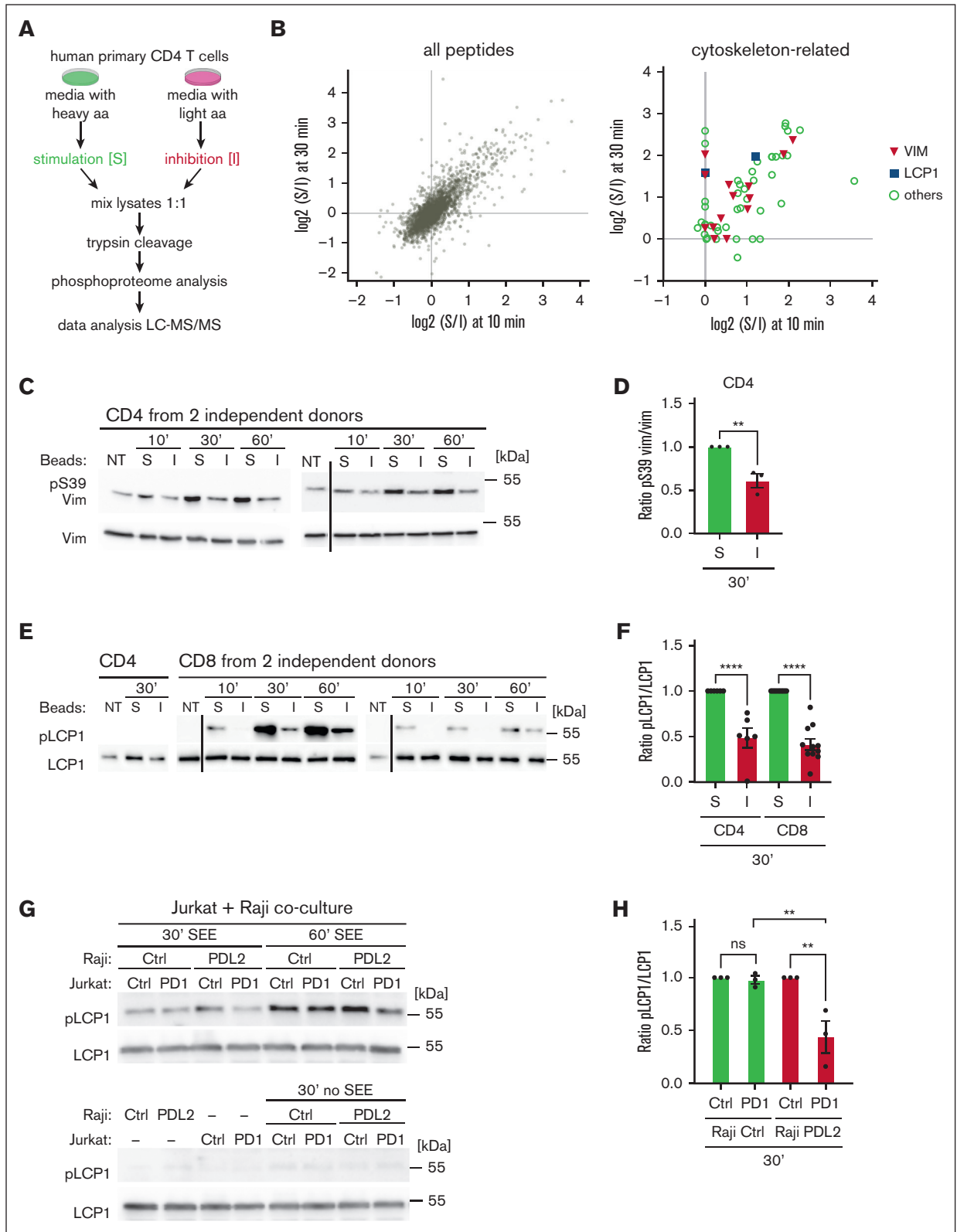


Figure 1. PD1 triggering induced a reduction in S/T phosphorylation of cytoskeleton-related proteins. (A) Scheme of the SILAC labeling and mass spectrometry approach used to identify PD1-mediated changes in the phosphoproteome of human primary CD4 T cells. Cells were labeled with heavy or light SILAC media for 2 weeks and treated for 10 or 30 minutes with beads coated with anti-CD3 and anti-CD28 antibodies in combination with TACI-Fc (stimulatory beads) or PDL1-Fc (inhibitory beads). After mixing, lysates were digested with trypsin and phosphorylated peptides were identified by LC-MS/MS analysis. (B) Graphs summarizing phosphorylation events that differed

In the tumor microenvironment, various strategies are at work to dampen T-cell activation, allowing tumor immune escape.⁷ The receptor programmed cell death protein 1 (PD1), upregulated on activated T cells, is 1 of the major coinhibitors of T-cell activation.⁸ PD1 can be triggered by 1 of its ligands, PD ligand 1 (PDL1) or PDL2, expressed by immune and nonimmune cells, including infected and cancer cells.⁹ Ligand-dependent engagement of PD1 leads to T-cell inhibition.¹⁰⁻¹² Therefore, the PD1/PDL1 axis has gained much attention as a drug target in antibody-based tumor immunotherapies. Therapeutic blockade of PD1 or PDL1 has become a first- or second-line therapy in the treatment of several cancers, such as non-small cell lung cancer (NSCLC), melanoma, Hodgkin lymphoma or advanced renal carcinoma.¹³⁻¹⁶ Despite significant advancements in these therapies, PD1 targeting fails to provide the desired outcome in a substantial number of patients. It is estimated that targeting PD1/PDL1 with PD1-specific (eg, nivolumab) or PDL1-specific (eg, atezolizumab) monoclonal antibodies, achieves response rates between 10% and 25% in bladder, gastric or ovarian cancer.¹⁷ A better understanding of the PD1-mediated intracellular mechanisms leading to T-cell inhibition would help to develop predictive biomarkers, enabling more precise stratification of patients expected to benefit from PD1-based immunotherapies.

The tyrosine phosphatases Src homology 2 domain-containing phosphatase 1 (SHP1) and SHP2 are signaling proteins that mediate PD1-dependent T-cell inhibition.¹⁸⁻²⁰ PD1 triggering leads, in presence of a simultaneous stimulatory trigger, to the Lck-mediated phosphorylation of tyrosine residues Y223 and Y248 of PD1, which in turn provide binding sites with partially overlapping binding specificity for SHP1 and SHP2, respectively.¹⁹⁻²³ The recruitment of SHP1/SHP2 to PD1 is thought to activate the phosphatases, causing dephosphorylation of tyrosine residues of membrane-proximal proteins required for T-cell activation, such as ZAP70 and CD28.^{18,21,24} However, T-cell activation relies not only on tyrosine phosphorylation of membrane-proximal proteins, but also on changes within the serine and threonine (S/T) phosphoproteome,²⁵ which have received less attention in the context of PD1-mediated T-cell inhibition.

Here, we show that PD1 triggering leads to dephosphorylation of cytoskeleton-related proteins that are substrates and/or binding partners of the S/T kinase PKC θ . We additionally identify PKC θ itself as a key target of PD1-induced, SHP1/SHP2-mediated tyrosine dephosphorylation and PD1-induced inhibition of IS formation. Furthermore, we demonstrate that the phosphorylation status of the cytoskeleton protein and PKC θ target vimentin is a

bona fide indicator of PD1 engagement. Finally, we provide evidence for an inverse correlation between the status of vimentin phosphorylation on S39 in T cells and the extent of PDL1 expression in human lung adenocarcinoma tissues. These findings identify a new aspect of PD1 signaling with potential relevance for biomarker development.

Materials and methods

Details on the cells, constructs, reagents, and assays used for this study are provided in the supplemental Material and Methods.

T-cell stimulation

For beads-mediated stimulation, Dynabeads M450Epoxy were coupled according to manufacturer's instructions with anti-CD3 ab (OKT3) at 5%, anti-CD28 ab (CD28.2) at 10% and TACI-Fc or PDL1-Fc at 85% of beads capacity to obtain stimulatory (S) or inhibitory (I) beads, respectively. TACI-Fc is a recombinant receptor whose ligands BAFF and APRIL are not expressed on T cells and served as a control protein. Cells were stimulated at a 1:3 (cell:bead) ratio for the indicated time points. If required, we prestimulated CD4 and CD8 T cells to increase PD1 surface expression with cross-linked anti-CD3 and anti-CD28 abs at 1 μ g/mL for 48 hours; we then washed and incubated the cells for 24 hours in 10% fetal calf serum/RPMI before beads-mediated stimulus. For stimulation of Jurkat cells or human primary T cells with Raji cells, the latter were incubated for 30 minutes with staphylococcal enterotoxin E (SEE) or with a mixture of SEA, SEB, and SEE at indicated concentrations. Raji cells were then mixed with Jurkat cells at a 1:1 ratio or with primary T cells at a 1:2 ratio for the time of stimulation. Cells were stimulated with cross-linked anti-CD3 and anti-CD28 abs or PMA (phorbol 12-myristate 13-acetate, 20 ng/mL) and ionomycin (1 μ M) for the indicated times and concentrations. Where indicated, cells were pretreated with the PKC θ inhibitor (2,4-diamino-5-nitropyrimidine) or the kinase C inhibitor BIM8 (bisindolylmaleimide VIII acetate) at indicated concentrations for 60 minutes at 37°C.

Labeling and conjugate formation

Jurkat and Raji cells were labeled with CMTMR (1 μ M) or CFSE (10 nM) \pm SEE, respectively, for 30 minutes at 37°C, then pelleted, resuspended at 10⁶ cells/mL in 10% fetal calf serum/RPMI-1640, mixed at a 1:1 ratio and incubated for 30 minutes (unless indicated otherwise) at 37°C to allow conjugate formation.

Figure 1 (continued) between stimulatory (S) and inhibitory (I) conditions. Left graph: all identified sites. Dots in the upper right quarter represent sites for which phosphorylation decreased upon PD1 triggering at both, the 10- and 30-minute time points. Right graph: only cytoskeleton-related proteins, including vimentin and LCP1. (C) Western blot analysis monitoring phosphorylation of S39 (pS39) of vimentin (Vim) in human primary CD4 T cells from 2 independent donors, left untreated (NT) or triggered for the indicated time points with S or I beads. Black vertical line indicates removal of an irrelevant lane. (D) Quantification of the experiments performed as in panel C: pS39 Vim levels were normalized to total Vim levels for the 30-minute condition for 3 independent experiments. (E) Western blot analysis monitoring phosphorylation of S5 of L-plastin (pLCP1) in human primary CD4 and CD8 T cells from 2 independent donors. Cells were left untreated (NT) or triggered for the indicated time points with S or I beads. Black vertical line indicates the cut of the image performed to remove 5-minute time point, which was not relevant for this figure. (F) Quantification of experiments performed as in panel E: pS5 LCP1 levels in CD4 (upper panel) and CD8 (lower panel) were normalized to total LCP1 levels for the 30-minute condition, for 6 and 11 independent experiments, respectively. (G) Western blot analysis monitoring phosphorylation of S5 of L-plastin (pLCP1) in Jurkat Ctrl cells or in Jurkat cells expressing WT PD1 (PD1) triggered for the indicated time points with Raji Ctrl cells or Raji PDL2 in presence or absence of SEE at 6 ng/mL. (H) Quantification of experiments performed as in panel G: pS5 LCP1 level in Jurkat cells was normalized to total LCP1 level for the 30-minute condition for 3 independent experiments. Graphs in panels D,F,H show mean value \pm SEM. Statistical analysis for graphs in panels D,F was performed using a 2-tailed, unpaired *t* test. Statistical analysis for graph in panel H was performed using 1-way ANOVA with Šidák's multiple comparisons test. *****P* < .0001; ****P* < .001; ***P* < .01. ANOVA, analysis of variance; SEM, standard error of the mean.

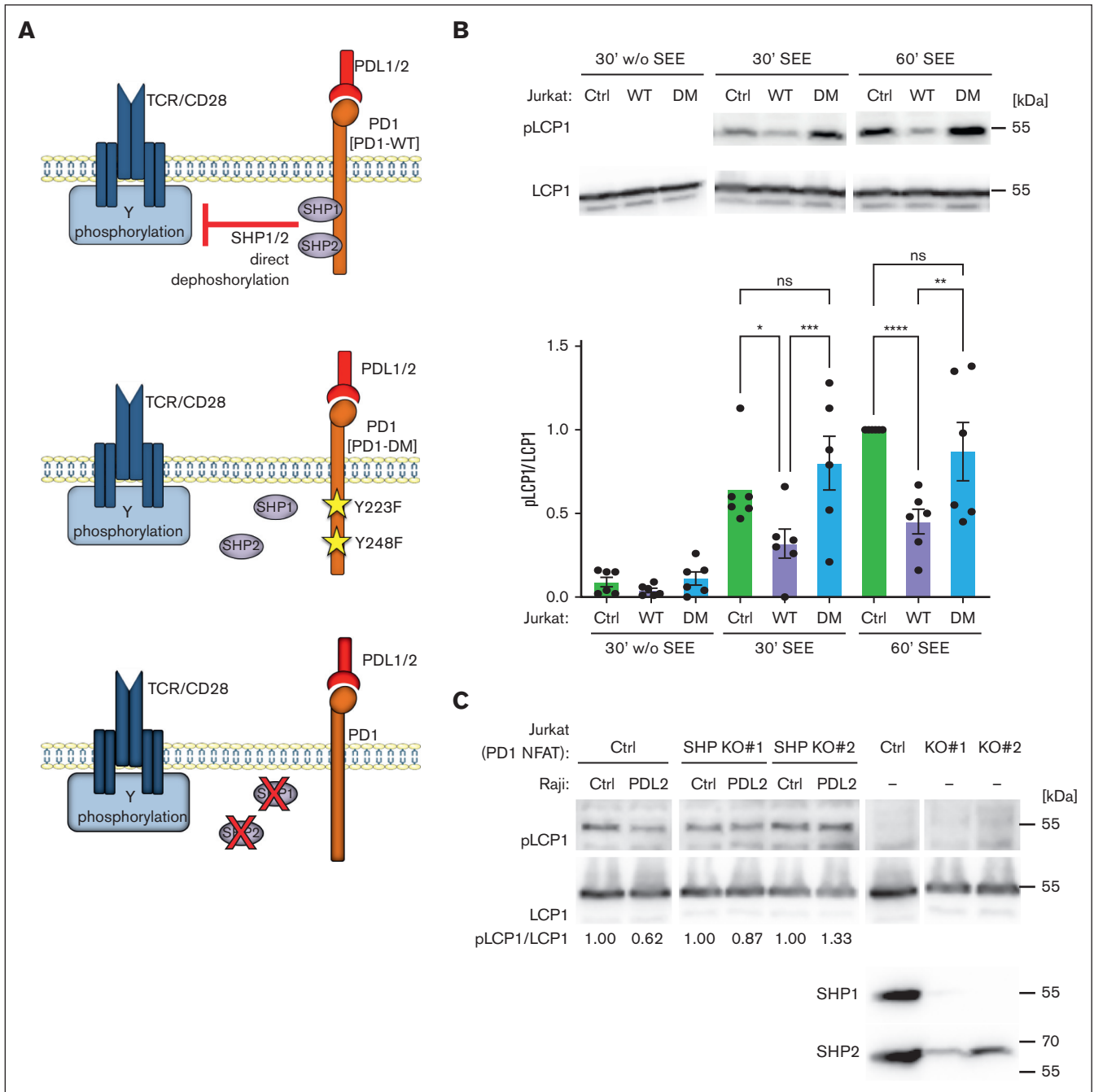


Figure 2. PD1-triggered inhibition of LCP1 phosphorylation is SHP1/SHP2-dependent. (A) Overview of the Jurkat cell lines used to assess the relevance of SHP1/2 phosphatases in the PD1-induced dephosphorylation of cytoskeleton proteins. Upper section: Ctrl cells expressing WT PD1. Middle section: Jurkat cells expressing PD1 DM, Y223F/Y248F, unable to bind SHP1/SHP2. Lower section: CRISPR/Cas9-mediated silencing of SHP1 and SHP2 in Jurkat-PD1-NFAT cells. (B) Upper panel: western blot monitoring phosphorylation of S5 of L-plastin (pLCP1) in the indicated cell lines. Jurkat-PD1 WT and Jurkat-PD1 DM cells were cocultured for the indicated times with PDL2-expressing Raji cells (Raji PDL2) in presence or absence of SEE at 6 ng/mL. Lower panel: quantification of experiments, pS5 LCP1 was normalized to total LCP1 for the 60-minute condition for 6 independent experiments. (C) Western blot monitoring phosphorylation of S5 of L-plastin (pLCP1) in 2 independent Jurkat-PD1-NFAT cell lines stably transduced with SHP1- and SHP2-specific CRISPR constructs and cocultured for 30 minutes with Raji Ctrl cells or Raji PDL2 in presence of SEE at 6 ng/mL. Representative data from 4 independent experiments.

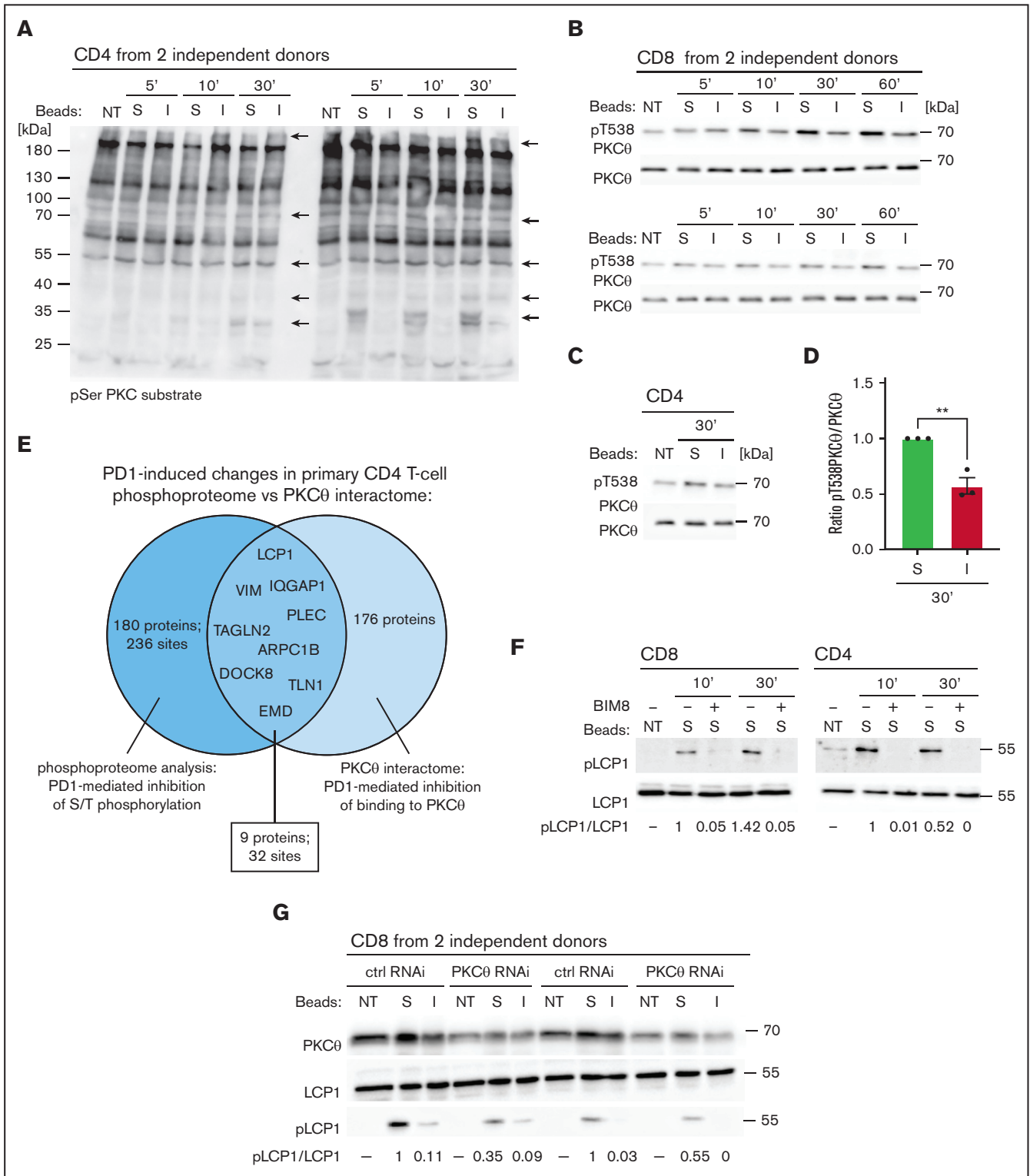


Figure 3. PD1 triggering inhibits binding and phosphorylation of proteins by PKCθ. (A) Western blot monitoring phosphorylation of PKC substrates on serine residues embedded within the pentapeptide motif K/R-X-pS-hydrophobic aa-K/R in lysates of human primary CD4 T cells from 2 independent donors. Cells were left untreated (NT) or triggered for the indicated time points with stimulatory (S) or inhibitory (I) beads. Arrows indicate protein bands that show reduced phosphorylation upon treatment with inhibitory beads. (B,C) Western blot monitoring PKCθ phosphorylation at T538 and total PKCθ levels in lysates of human primary CD8 from 2 independent donors (B) and CD4 (C) T cells. Cells were left NT or triggered for the indicated time points with S or I beads. (D) Quantification of experiments performed as in panels B,C: pT538 PKCθ levels in human primary T cells were normalized to total PKCθ levels for the 30-minute condition for 3 independent experiments. Mean values ± SEM. Statistical analysis was performed with a 2-tailed,

Immunocytochemistry staining and confocal microscopy

Cells were layered on polylysine coverslips, centrifuged (1 minute, 450 g), incubated on ice for 5 minutes, fixed with 4% paraformaldehyde (PFA) for 15 minutes on ice and quenched with 50 mM NH₄Cl for 10 minutes. Cells were treated with 0.05% saponin/0.2% bovine serum albumin in phosphate-buffered saline for 15 minutes. Fc receptors were blocked using Fc receptor blocking solution. Immunostainings were performed with indicated antibodies and samples were mounted in medium with DAPI to stain nuclei. Images were acquired using a Zeiss LSM880 confocal microscope with EC Plan Neofluar 40x/1.3 NA and EC Plan Neofluar 63x/1.25 NA oil immersion objectives. For quantification of confocal images, the total fluorescence intensity was measured in whole cells or IS regions of the focal plane using Fiji software. Red-green-blue (RGB) intensity plot was obtained using ImageJ plugin RGB Profiler.

Image stream

Analysis was conducted using an ImageStream X MKII (ISx) system. Up to 40 000 cell events per sample were collected at 60x magnification.

Lung adenocarcinoma samples

Ten lung adenocarcinomas cases (5 PDL1^{low} and 5 PDL1^{high}) were collected upon receiving consent at the Centre Hospitalier Universitaire Vaudois and anonymized, followed by 5-plex staining of CD3, PD1, pan-cytokeratin (PanCK), pS39Vimentin, and PDL1.

Western blots

Cells were lysed in SDS-PAGE (sodium dodecyl sulfate-polyacrylamide gel electrophoresis) protein sample buffer and boiled at 96°C for 10 minutes, followed by analysis on high-resolution SDS-PAGE and immunoblot as described.²⁶

Phosphoproteome analysis

Cells were cultured in stable isotope labeling by amino acids in cell culture (SILAC) medium for more than 2 weeks, stimulated and lysed in 8M urea and digested essentially as described.²⁷ Phosphopeptide enrichment was performed as described.²⁸ Details on liquid chromatography-tandem mass spectrometry (LC-MS/MS) analysis and data processing are described in the supplemental Material and Methods.

PKCθ interactome

PKCθ immunoprecipitates were analyzed by Coomassie blue staining, gel lanes were excised into 6 equal regions and in-gel digested with trypsin (Promega) as described.²⁹ LC-MS/MS

analysis was carried out on a Q-exactive Plus orbitrap mass spectrometer (for details see supplemental Material and Methods).

Blood samples from healthy, informed, and consenting human donors were obtained from Interregional Blood Transfusion SRC Ltd (Epalinges, Switzerland). Lung adenocarcinomas cases (5 PDL1^{low} and 5 PDL1^{high}) were collected upon consent at the Centre Hospitalier Universitaire Vaudois and were anonymized.

Results

PD1 inhibits S/T phosphorylation of cytoskeleton-related proteins in primary human T cells

As an experimental system to identify PD1-specific changes in the phosphoproteome, we used primary human T cells in which PD1 expression was induced by prestimulation with cross-linked stimulatory anti-CD3/CD28 antibodies (supplemental Figure 1A). PD1 expression was typically at the highest 48 hours after stimulation, as previously reported.³⁰ To assess the functionality of PD1, T cells were then incubated with dynabeads, coupled with anti-CD3 and anti-CD28 antibodies,¹² together with recombinant PDL1-Fc (for inhibitory beads), or TACI-Fc protein (for stimulatory beads). Compared with stimulatory beads, inhibitory beads efficiently impaired extracellular signal-regulated kinase 1/2 phosphorylation (supplemental Figure 1B) and IL-2 secretion in CD4 and CD8 T cells (supplemental Figure 1C-D).

Next, we treated PD1⁺ primary human CD4 T cells with stimulatory vs inhibitory beads for 10 and 30 minutes and monitored differences in the total phosphoproteome (Figure 1A). For this, cells were grown under conditions of SILAC, and labeling efficiency (not shown) and T-cell responsiveness were verified prior to the experiment (supplemental Figure 1E). Using mass spectrometry, we identified and quantified over 6000 phosphorylation sites across the 2 time points (Figure 1B, left panel; supplemental Table 1; all phosphosites). Of these, 278 sites showed significant changes, when comparing inhibitory to stimulatory conditions (supplemental Table 1; significant phosphosites). Of note, we identified a PD1-induced decrease in phosphorylation of 60 sites within prominent cytoskeleton components or regulators (Figure 1B, right panel; supplemental Table 2). These included the intermediate filament protein vimentin, previously identified as a PKCθ substrate,³¹ the actin-bundling protein L-plastin (also called lymphocyte cytosolic protein, LCP1),^{32,33} previously reported to undergo phosphorylation upon TCR/CD28 costimulation,³⁴ and other actin cytoskeleton regulators (Figure 1B, right panel; supplemental Table 2). This suggests that PD1 promotes T-cell exhaustion, at least in part, through effects on cytoskeleton rearrangements that are important for IS formation.^{5,6,35}

Figure 3 (continued) unpaired *t* test. ***P* < .01. (E) Venn diagram graphically representing results of the PKCθ interactome and phosphoproteome analyses: 171 proteins underwent a significant PD1-mediated reduction in serine or threonine phosphorylation (dark blue circle), 253 proteins bound less well or did not bind to PKCθ upon PD1 triggering (light blue circle). The overlapping section contains 9 cytoskeleton proteins that show a significant decrease in serine phosphorylation and decreased binding to PKCθ upon PD1 triggering compared with the stimulating condition. (F) Western blot monitoring the effect of pretreatment with the pan-PKC inhibitor BIM8 on the phosphorylation of S5 of L-plastin (pLCP1) in human primary CD4 and CD8 T cells. Cells were pretreated as indicated for 1 hour, followed by triggering with S beads for the indicated times. Two representative blots of 3 independent experiments are shown. Densitometry analysis: the relative ratio of pLCP1 to total LCP in the samples is indicated below. (G) Western blot monitoring phosphorylation of S5 of L-plastin (pLCP1) in human primary CD8 T cells from 2 independent donors, nucleoporated with PKCθ-specific or Ctrl siRNAs. Seventy-two hours after nucleoporation, cells were triggered for 30 minutes with S or I beads. The relative ratio of pLCP1 to total LCP in the samples is indicated below.

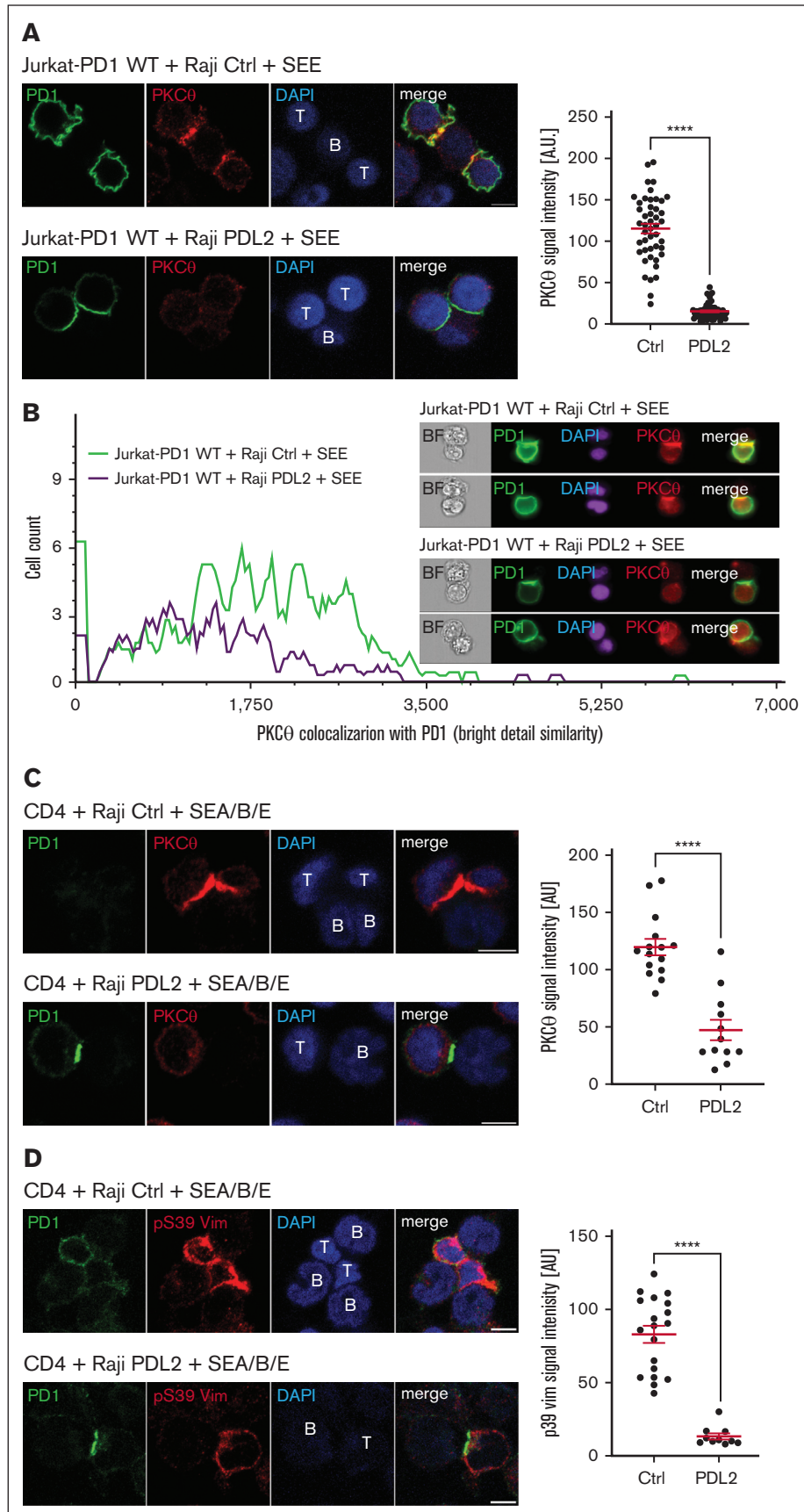


Figure 4.

PD1 engagement inhibits serine phosphorylation of vimentin and L-plastin

Next, we validated our phosphoproteome data using commercial antiphospho-Serine (pS) antibodies, available for the PD1-targeted phosphorylation sites identified here, pS39 and pS72 of vimentin and pS5 of LCP1. These revealed efficient induction of vimentin and LCP1 phosphorylation upon various conditions of primary human CD4 T-cell activation (supplemental Figure 2A). Although resting cells exhibited some constitutive vimentin phosphorylation at S39 and S72, phosphorylation at S39 was enhanced by stimulatory beads, while inhibitory beads induced a decrease of both, pS39 and pS72, compared with stimulatory beads (Figure 1C-D; supplemental Figure 2B-C). Moreover, we observed a strong PD1-mediated inhibition of LCP1 S5 phosphorylation in CD4 and CD8 T cells (Figure 1E-F). We confirmed our findings using PD1-transduced wild-type Jurkat T cells (Jurkat-PD1 WT), which were cocultured with mock-transduced or PDL1- or PDL2-transduced Raji cells, in the presence or absence of the superantigen SEE (supplemental Figure 3A-B).^{21,36} In this setting, PD1 engagement strongly decreased SEE-dependent IL-2 secretion (supplemental Figure 3C) and LCP1 S5 phosphorylation (Figure 1G-H). No such effect was seen on Jurkat cells lacking PD1 expression. Thus, PD1 triggering inhibits S/T phosphorylation of multiple cytoskeleton-related proteins in human primary T cells and Jurkat T cells.

PD1-induced inhibition of LCP1 phosphorylation depends on SHP1 and SHP2

The tyrosine phosphatases SHP1 and SHP2 contribute to PD1-mediated T-cell inhibition, even if their individual contributions remain somewhat controversial.^{19-21,37-40} To assess if these phosphatases play a role in the PD1-induced dephosphorylation of cytoskeleton proteins, we developed 2 strategies (Figure 2A). First, we generated Jurkat cell lines expressing either PD1 WT or a PD1 double mutant (PD1 DM) for both SHP1 and SHP2 binding sites, Y223F and Y248F (Figure 2A, middle panel; supplemental Figure 3B). Second, we stably silenced SHP1 and SHP2 expression in a commercially available Jurkat cell line expressing PD1 and an NFAT reporter (Jurkat-PD1 NFAT cells) (Figure 2A, lower panel). For both strategies, we verified surface levels of PD1, CD3 and CD28 (supplemental Figures 3B and 4). Triggering of Jurkat cells

with Raji PDL2 cells inhibited LCP1 S5 phosphorylation in Jurkat-PD1 WT, but not Jurkat-PD1 DM or Jurkat control (Ctrl) cells, suggesting that PD1-mediated recruitment of SHP1 and SHP2 was necessary for LCP1 dephosphorylation (Figure 2B). Similarly, CRISPR/Cas9-mediated silencing of both, SHP1 and SHP2 prevented PD1-induced dephosphorylation of LCP1 in Jurkat-PD1 NFAT cell lines (Figure 2C). Thus, PD1 triggering inhibits LCP1 phosphorylation in a SHP1/SHP2-dependent manner.

PD1 inhibits PKC θ -mediated binding and phosphorylation of cytoskeleton-related proteins

PKC family members regulate phosphorylation and activation of various cytoskeletal compounds,⁴¹⁻⁴³ including vimentin.³¹ These findings, together with a previous report describing PD1-mediated inhibition of PKC θ threonine phosphorylation,²⁴ allows us to hypothesize that PKC θ might be a major mediator of the observed PD1-induced reduction in the S/T phosphoproteome. We, thus, assessed the total phosphorylation levels of PKC θ substrates in primary CD4 T cells treated with stimulatory or inhibitory beads by Western blotting, using an anti-pS PKC substrate antibody (Figure 3A). This revealed a PD1-induced decrease of phosphorylation of multiple proteins. Next, we tested the status of PKC θ phosphorylation at T538, a surrogate marker for PKC θ kinase activation.⁴⁴ In unstimulated T cells, we observed a basal level of T538 phosphorylation of PKC θ . Addition of stimulatory beads led to a further increase in phosphorylation for at least 60 minutes, and this was inhibited by PD1 triggering in both CD8 and CD4 T cells (Figure 3B-D). Next, we performed an MS-based analysis of PKC θ binding partners in CD4 T cells triggered with stimulatory or inhibitory beads for 10 minutes. PKC θ was immunoprecipitated (IP) with comparable efficiency in both conditions (supplemental Table 3). When using a cutoff of at least 4 spectral counts/protein in 1 of the conditions for each identified target, we identified 176 proteins, including 33 cytoskeleton-related proteins, whose interaction with PKC θ was severely diminished upon PD1 triggering (supplemental Table 3; cytoskeleton-related proteins). Among these were 9 proteins, including vimentin and LCP1, who showed a diminished interaction with PKC θ and a correlating decrease in S/T phosphorylation upon PD1 triggering (Figure 3E; supplemental Tables 1 and 3). Finally, we monitored the effects of pretreatment with the pan-PKC inhibitor BIM8 or of PKC θ silencing on the status of LCP1 pS5 in stimulated primary T cells.

Figure 4. PD1 triggering affects PKC θ recruitment and vimentin phosphorylation at the IS. (A) Left: immunofluorescent labeling of PD1 and PKC θ upon 60 minutes of coculture of Jurkat-PD1 WT cells with Raji Ctrl cells (upper panel) or PDL2 expressing Raji cells (lower panel), preincubated with 6 ng/mL of SEE and mixed with Jurkat-PD1 WT cells at a 1:1 ratio. Right: quantification of the PKC θ signal intensity in Jurkat cells within proximity of the T and B cell interface from 1 experiment. Representative results of 4 independent experiments are shown. Each dot represents a value from 1 Jurkat cell, 46 and 56 cells were quantified, respectively. (B) ImageStream-based quantification of the colocalization between PD1 and PKC θ in Jurkat-PD1 WT cells cocultured for 60 minutes with Raji Ctrl or Raji PDL2 cells, preincubated with 6 ng/mL of SEE and mixed with Jurkat-PD1 WT cells at a 1:1 ratio. Upon fixation and permeabilization, samples were stained for PKC θ , PD1 and nuclei (DAPI) and analyzed by ImageStream flow cytometry. Left: histogram measuring the extent of signal overlap between PKC θ and PD1, with PD1 signal in the IS used as a mask; right: examples of images acquired. Representative results of 2 independent experiments are shown. (C) Left: immunofluorescent labeling of PD1 and PKC θ upon 30 minutes of coculture of human primary CD4 T cells with Raji Ctrl cells (upper panel) or Raji PDL2 cells (lower panel). Raji cells were preincubated with 1 ng/mL of SEA/SEB/SEE and mixed with CD4 cells at a 1:2 (Raji:T cells) ratio. Images shown are from a single Z plane, which likely accounts for the concentration of staining in the T cell in the absence of PDL2 ligation, whereas the signal is weaker in the Raji PDL2 condition (bottom panel). Right: quantification of the PKC θ signal intensity in T cells within proximity of the T cell-B cell interface from 1 experiment. Representative results of 3 independent experiments are shown. Each dot represents a value from 1 primary T cell, 15 and 12 cells were quantified, respectively. (D) Left: immunofluorescent labeling of PD1 and pS39 Vim upon 60 minutes of coculture of human primary CD4 T cells with Raji Ctrl cells (upper panel) or Raji PDL2 cells (lower panel). Raji cells were preincubated with 6 ng/mL of SEE and mixed with Jurkat-PD1 WT cells at a 1:2 (Raji:T cells) ratio. Right: quantification of the total pVim39 signal intensity in T cells from 1 experiment. Representative results of 3 independent experiments are shown. Each dot represents a value from 1 primary T cell, 19 and 10 cells were quantified, respectively. Scale bar: 5 μ m (panels A,C-D). Graphs in panels A,C-D show mean value \pm SEM. Statistical analysis was performed using a 2-tailed, unpaired t-test. **** $P < .0001$.

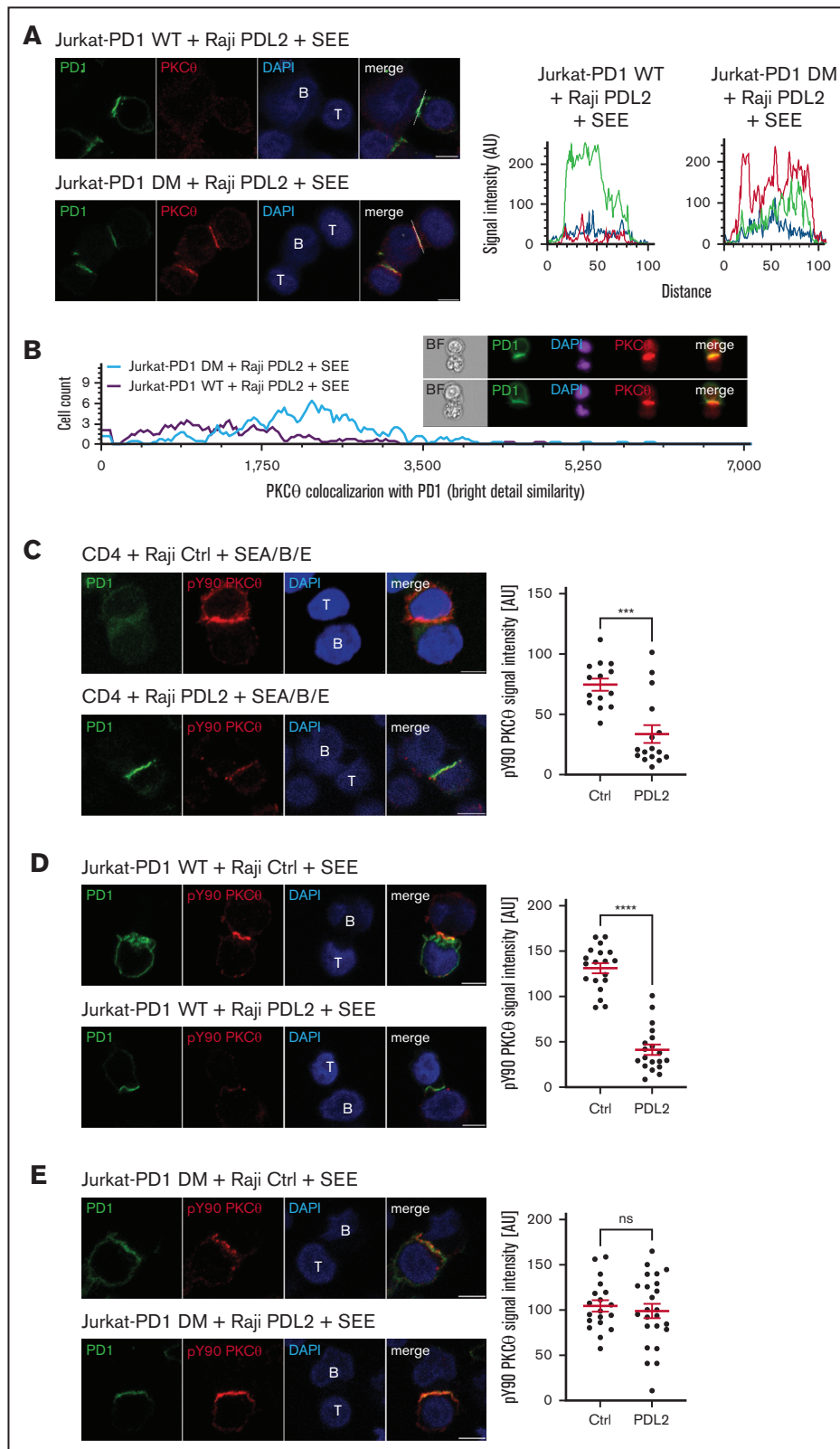


Figure 5. PD1-induced inhibition of PKC θ localization to the IS is SHP1/SHP2-dependent. (A) Left: immunofluorescent labeling of PD1 and PKC θ of Jurkat-PD1 WT cells (upper panel) and Jurkat-PD1 DM cells (lower panel) upon 60 minute of coculture with Raji PDL2 cells, preincubated with 6 ng/mL of SEE and mixed with Jurkat cells at a 1:1 ratio. Right: representative histogram of the colocalization profile prepared with RGB profiler plugin of ImageJ. Representative images of 3 independent experiments are shown. (B) ImageStream-based quantification of the colocalization between PD1 and PKC θ in Jurkat-PD1 WT cells and Jurkat-PD1 DM cells cocultured for 60 minutes with Raji PDL2

Pretreatment with BIM8 completely blocked stimulation-induced LCP1 S5 phosphorylation in CD4 and CD8 T cells (Figure 3F). Similarly, pretreatment of Jurkat-PD1 NFAT and Jurkat-PD1 WT cells with BIM8 or a PKC θ inhibitor blocked stimulation-induced LCP1 S5 phosphorylation (supplemental Figure 5). We also observed a marked decrease in LCP1 S5 phosphorylation in stimulated, PKC θ -silenced primary T cells compared with control cells (Figure 3G). Thus, LCP1 is a direct or indirect target of PKC θ -mediated phosphorylation.

Collectively, these findings suggest that PD1 triggering inhibits the activation of PKC θ , as well as the PKC θ -dependent physical recruitment and phosphorylation of cytoskeleton-related proteins, including vimentin and LCP1.

PD1 inhibits PKC θ localization to the forming IS

Next, we investigated the consequences of PD1 triggering on the known IS recruitment of PKC θ .⁴⁵ We observed a clear translocation of PKC θ to the forming IS in Jurkat-PD1 WT cells upon coculture with Raji Ctrl cells (Figure 4A, upper panels), but not with Raji PDL2 cells, where PKC θ remained dispersed, with little or no enrichment at the IS (Figure 4A, lower panels). Importantly, PD1 triggering also led to strong accumulation of PD1 at the contact zone, as described.¹⁹ We next quantified the effect of PD1 on PKC θ recruitment to the IS using ImageStream (Figure 4B) gating on clusters of at least 2 cells, including 1 positive for PD1 staining (supplemental Figure 6). Quantification of the PKC θ and PD1 signal overlap within the synapse region confirmed that the PKC θ signal was reduced when Jurkat-PD1 cells were triggered with PDL2-expressing Raji cells (Raji PDL2), whereas PD1 accumulated within the IS (Figure 4B).

We also assessed the effect of PD1 engagement on the subcellular localization of PD1 and PKC θ in primary human CD4 T cells upon coculture with Raji Ctrl vs Raji PDL2 cells presenting the superantigens SEA, SEB, and SEE. Coculture with Raji PDL2 cells led to a reduced IL-2 response in this system (supplemental Figure 7) and resulted in accumulation of PD1, but not of PKC θ at the IS (Figure 4C). Moreover, superantigen stimulation induced a pS39 vimentin signal at the IS, which was almost totally abrogated by PD1 engagement (Figure 4D). ImageStream analysis confirmed PD1-induced inhibition of Vimentin phosphorylation (supplemental Figure 8). Thus, PD1 triggering leads to enrichment of PD1 at the IS, and prevents PKC θ recruitment and substrate phosphorylation at the IS.

PD1 inhibits IS recruitment and Y90 phosphorylation of PKC θ in a SHP1/2-dependent manner

To assess the relevance of PD1-induced SHP1/2 activation for IS recruitment of PKC θ , we compared the pattern of PKC θ localization in Jurkat cells expressing WT PD1 or its SHP1/SHP2 binding-deficient DM version, upon triggering with Raji PDL2 cells (Figure 5A). In Jurkat-PD1 WT cells, PKC θ was dispersed throughout the cell without any clear enrichment pattern, as observed before (Figure 4A). In contrast, in Jurkat-PD1 DM cells triggered with Raji PDL2 cells, PKC θ was concentrated within the Jurkat-Raji interface and colocalized with PD1 DM, which still enriched within the same interface (Figure 5A, RGB profile histogram). Triggering of Jurkat-PD1 WT or DM cells in the absence of PD1 engagement resulted in comparable enrichment of PKC θ within the IS (supplemental Figure 9).

We also assessed the overlap of PKC θ with PD1 signals in the IS using ImageStream (Figure 5B). As evident from the histogram analysis, the intensity of the PKC θ signal colocalized with PD1 was considerably higher in Jurkat-PD1 DM cells than in Jurkat-PD1 WT cells upon triggering with Raji-PDL2 cells (Figure 5B, plot for Jurkat-PD1 WT cells is the same as shown in Figure 4B). Thus, signaling through the PD1 SHP1/SHP2 binding sites is required to inhibit recruitment of PKC θ to the IS.

As Lck-mediated phosphorylation of Y90 of PKC θ is required for its targeting to the IS,^{46,47} we next monitored its phosphorylation status under stimulatory vs inhibitory conditions using a PKC θ pY90-specific antibody. Superantigen-mediated stimulation of CD4 T cells with Raji Ctrl cells led to a strong, IS-localized pY90 PKC θ signal (Figure 5C), which was greatly reduced upon PD1 engagement. Moreover, PKC θ Y90 phosphorylation was inhibited by WT PD1, but not by PD1 DM (Figure 5D-E). Indeed, for Jurkat-PD1 DM cells, the localization and intensity of PKC θ Y90 phosphorylation was comparable between stimulatory and inhibitory conditions (Figure 5E). Altogether, these data suggest that the initial, PD1- and SHP1/SHP2-dependent Y90 dephosphorylation of PKC θ represents a crucial link to the subsequent alterations in S/T-phosphorylation events at the IS.

PD1 engagement inhibits formation of the IS

We reasoned that the observed PD1-mediated inhibition of localized phosphorylation of cytoskeleton proteins should alter cytoskeleton plasticity and translate to an inhibition of the formation of the IS. Therefore, we measured the size of IS upon coculture of

Figure 5 (continued) cells. Raji PDL2 cells were preincubated with 6 ng/mL of SEE and mixed with Jurkat cells at 1:1 ratio. Upon fixation and permeabilization, samples were stained for PKC θ , PD1, and nuclei (DAPI) and analyzed by Amnis Image Stream imaging flow cytometry. Left: histogram measuring the extent of signal overlap between PKC θ and PD1 with PD1 signal in the IS used as a mask; right: examples of images acquired. Representative results of 2 independent experiments are shown. (C) Left: immunofluorescent labeling of PD1 and pY90 PKC θ of human primary CD4 T cells upon 60 minute of coculture with Raji Ctrl cells (upper panel) or Raji PDL2 cells (lower panel). Raji cells were preincubated with 1 ng/mL of SEA/SEB/SEE and mixed with CD4 cells at a 1:2 (Raji:T cells) ratio. Right panel: quantification of total pY90 PKC θ signal intensity in T cells from 1 experiment. Representative results of 3 independent experiments are shown. Each dot represents the value from 1 primary T cell, 14 and 16 cells were quantified, respectively. (D) Left: immunofluorescent labeling of PD1 and pY90 PKC θ of Jurkat-PD1 WT cells upon 30 minutes of coculture with Raji Ctrl cells (upper panel) or Raji PDL2 cells (lower panel). Raji cells were preincubated with 6 ng/mL of SEE and mixed with Jurkat-PD1 WT cells at 1:1 ratio. Right panel: quantification of total pY90 PKC θ signal intensity in Jurkat-PD1 WT cells. Representative results of 3 independent experiments are shown. Each dot represents a value from 1 Jurkat cell, 19 and 19 cells were quantified, respectively. (E) Left: immunofluorescent labeling of PD1 and pY90 PKC θ of Jurkat-PD1 DM cells upon 60 minute of coculture with Raji Ctrl cells (upper panel) or Raji PDL2 cells (lower panel). Raji cells were preincubated with 6 ng/mL of SEE and mixed with Jurkat-PD1 DM cells at 1:1 ratio. Right panel: quantification of total pY90 PKC θ signal intensity in Jurkat-PD1 DM cells. Representative results of 3 independent experiments are shown. Each dot represents a value from 1 Jurkat cell, 19 and 24 cells were quantified, respectively. Scale bar, 5 μ m. Graphs in panels C-E show mean value \pm SEM. Statistical analysis was performed using a 2-tailed, unpaired *t* test. *****P* < .001; ****P* < .001; ns, not significant.

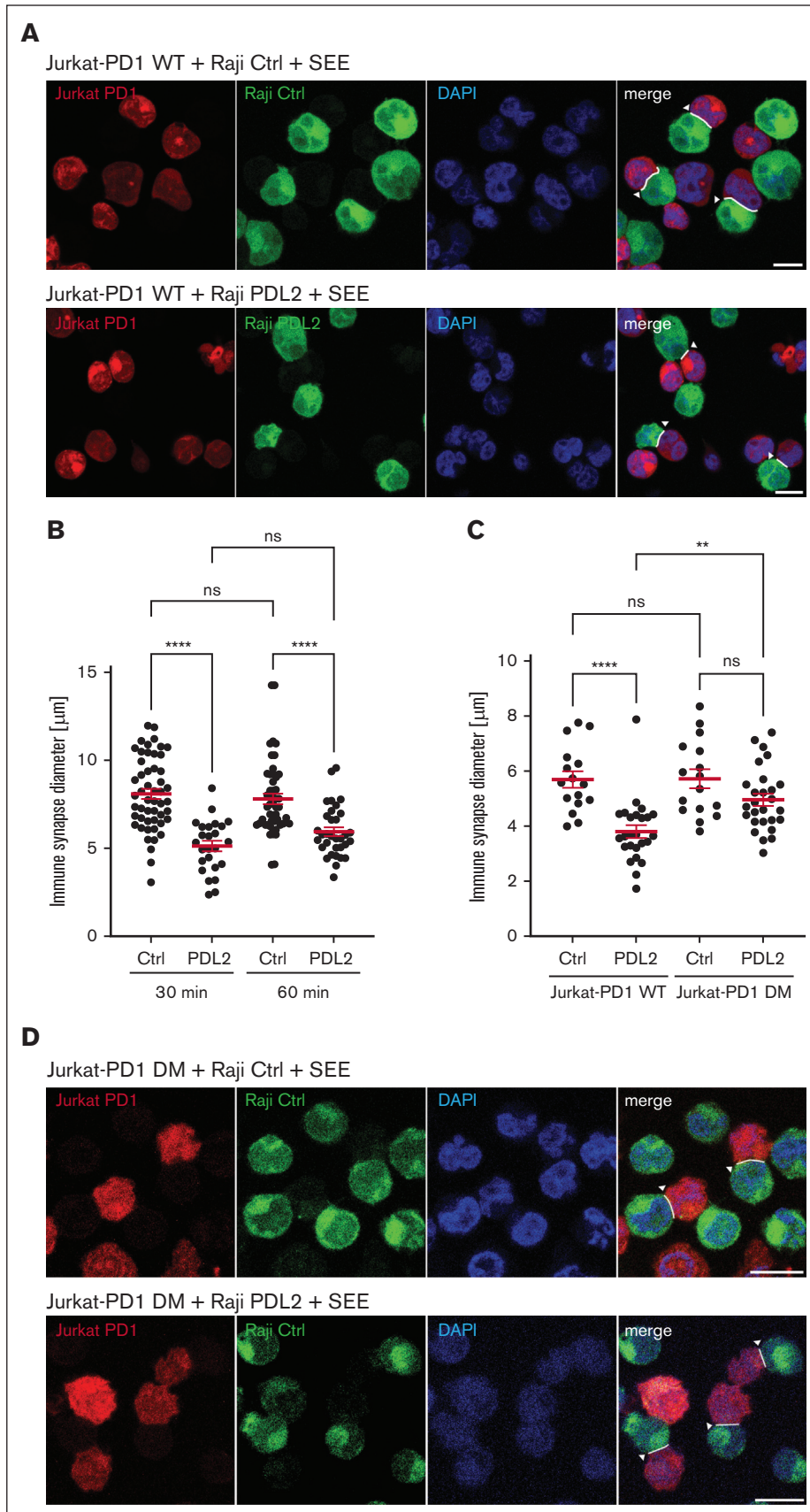


Figure 6.

Jurkat-PD1-NFAT cells with Raji Ctrl or Raji PDL2 cells for 30 or 60 minutes. PD1 triggering with PDL2 led to formation of IS that were significantly reduced in size (Figure 6A-B). Importantly, no significant effect on IS size was observed when Jurkat-PD1 DM cells were triggered with Raji PDL2 cells (Figure 6C-D). We also assessed whether PD1 engagement affected the frequency of conjugate formation between Jurkat and SEE-loaded Raji cells by flow cytometry (data not shown). However, the low concentration of SEE required to allow efficient PD1-mediated T-cell inhibition was not sufficient to trigger robust formation of conjugates stable enough for analysis by flow cytometry. Together with our biochemical data, these findings suggest that PD1 inhibits T-cell activation, at least in part, by preventing the synaptic translocation and activation of PKC θ and its targeting of cytoskeleton substrates required for the extension of the size of the IS.

Presence of PDL1 negatively correlates with vimentin phosphorylation in T cells in human lung adenocarcinoma

While most of the described PD1-induced changes in T-cell signaling are phospho-tyrosine-based and thus rather short lasting,²¹ the stimulation-induced phosphorylation of LCP1 and vimentin and their PD1-mediated dephosphorylation were still detectable 24 hours after T-cell triggering (Figure 7A). This prompted us to investigate a potential inverse correlation between vimentin phosphorylation in T cells and PDL1 expression on cancer cells in lung adenocarcinoma—a subtype of NSCLC responsive to targeting the PD1-PDL1 axis.^{48,49} We stained a total of 10 human biopsy samples, characterized by either low or high PDL1 expression in cancer cells, for PanCK (present in tumor cells), CD3, PD1 and vimentin pS39. In PDL1^{low} tumor samples, a significant proportion of the CD3⁺PD1⁺ T cells stained positive for vimentin pS39. In contrast, this proportion was low or undetectable in PDL1^{high} tumors (Figure 7B-C, left panel). Similar observations were made when all CD3⁺ T cells were analyzed (Figure 7C, right panel). For overall numbers of CD3⁺ or CD3⁺PD1⁺ cells in the tumor or stroma regions, we did not notice a consistent correlation of T-cell numbers with PDL1 expression in the tumors (supplemental Figure 10). These data suggest that low or absent pSer39 vimentin staining might provide a useful readout to monitor functional PD1 engagement in tumor-infiltrating T cells.

Discussion

Here, we provide several lines of evidence for a crucial role of PD1-mediated PKC θ inhibition in the control of TCR/CD28-mediated IS formation and T-cell activation. We identified decreased phosphorylation of multiple cytoskeleton-related proteins as a major outcome

of PD1-induced T-cell inhibition. Second, we identified PKC θ as the PD1 target and master kinase required for the recruitment and phosphorylation of 9 of these proteins. Third, we provided a link between transient PD1-induced changes in the Y-phosphoproteome and long-term changes in S/T-phosphorylation of cytoskeleton-related proteins and IS formation. Finally, we propose PD1-controlled phosphorylation of vimentin as a potential marker for assessing T-cell effector functions in human lung cancer samples.

Importantly, our discoveries are based on an unbiased phosphoproteomics approach, performed on human primary CD4 T cells in the background of suboptimal CD3/CD28 stimulation, which likely allowed for optimal detection of PD1-mediated inhibitory effects. Inclusion of CD28 triggering was paramount for our study, because CD28 signaling is required for full T-cell activation, including PKC θ activation and actin cytoskeleton remodeling.⁵⁰ In addition, CD28 signaling is important for both, PD1-induced T-cell inhibition and effective rescue of T-cell exhaustion via PD1-targeting therapies.^{21,51,52} Our study, therefore, provided mechanistic insights into PKC θ -dependent cytoskeleton changes that go beyond previous phospho-proteomics studies, which used Jurkat cells stimulated with anti-CD3 alone, likely not engaging PKC θ efficiently.⁵³ The latter revealed mainly CD3-driven alterations in tyrosine phosphorylation of cytoskeleton proteins and no obvious effects of PD1 on an in silico predicted PKC θ substrate profile.

We also identified a requirement for SHP1 and SHP2 in the PD1-mediated inhibition of Y-phosphorylation and IS recruitment of PKC θ , and the phosphorylation of the PKC θ substrate LCP1. These findings support a model in which PD1 inhibits cytoskeleton rearrangements, directly or indirectly, by SHP1/SHP2-dependent dephosphorylation of PKC θ and its cytoskeleton targets (supplemental Figure 11). Of note, PD1 accumulation at the IS did not depend on its immunoreceptor tyrosine-based inhibitory motif and immunoreceptor tyrosine-based switch motif, it must, thus, rely on signaling events that are independent of SHP1/SHP2 binding. The latter may indeed be responsible for the recently reported, SHP1/2-independent effects of PD1 on the actin cytoskeleton,⁵⁴ which likely synergizes with the PD1-mediated, SHP1/2- and PKC θ -dependent inhibition of IS formation that we report here.

Among the cytoskeleton proteins whose serine phosphorylation was decreased upon PD1 engagement, we validated LCP1 S5, vimentin S39 and S72 using commercial antibodies. The actin-binding protein LCP1 is known to be phosphorylated on S5 in activated T cells, which affects the formation of high affinity clusters of the adhesion molecule LFA1 within the IS.³⁴ Our data suggest a role for PKC θ in LCP1 phosphorylation and identify S5 of LCP1 as a target of PD1-mediated inhibition. Vimentin has been previously proposed to be a substrate and binding partner of PKC θ . Indeed,

Figure 6. PD1 triggering decreases IS size through inhibition of PKC θ recruitment. (A) Assessment of the effect of PD1 triggering on the size (maximal diameter of the contact zone) of the IS. Jurkat-PD1-NFAT cells (labeled with CMTMR) were incubated with Raji Ctrl and Raji PDL2 cells (labeled with CFSE in presence of 6 ng/mL SEE), at a 1:1 cell ratio for 30 minutes at 37°C to facilitate IS formation. Image data from representative experiment, highlighting quantified IS by white arrowheads. Representative images of 2 independent experiments are shown. (B-C) Quantification of the size of the IS formed as described in panel A, using Jurkat-PD1-WT or DM cells (B) or Jurkat-PD1-WT cells, at different time points of incubation with Raji Ctrl and Raji PDL2 cells (C). Representative results of 2 and 3 independent experiments, respectively, are shown. Each dot represents a value from 1 Jurkat cell, (B) 51, 26, 50 and 33 cells; (C) 16, 25, 16 and 27 cells were quantified, respectively. (D) Assessment of the effect of PD1 triggering on the size (maximal diameter of the contact zone) of the IS. Jurkat-PD1-WT and Jurkat-PD1-DM cells (labeled with CMTMR) were incubated with Raji PDL2 cells (labeled with CFSE in presence of 6 ng/mL SEE), at a 1:1 cell ratio for 30 minutes at 37°C to facilitate IS formation. Image data from representative experiments, highlighting quantified IS by white arrowheads. Representative images of 3 independent experiments are shown. Scale bar, 10 μ m. Graphs in panels B-C show mean value \pm SEM. Statistical analysis was performed using 1-way ANOVA with Šidák's multiple comparisons test. **** $P < .0001$; ** $P < .01$; ns, not significant.

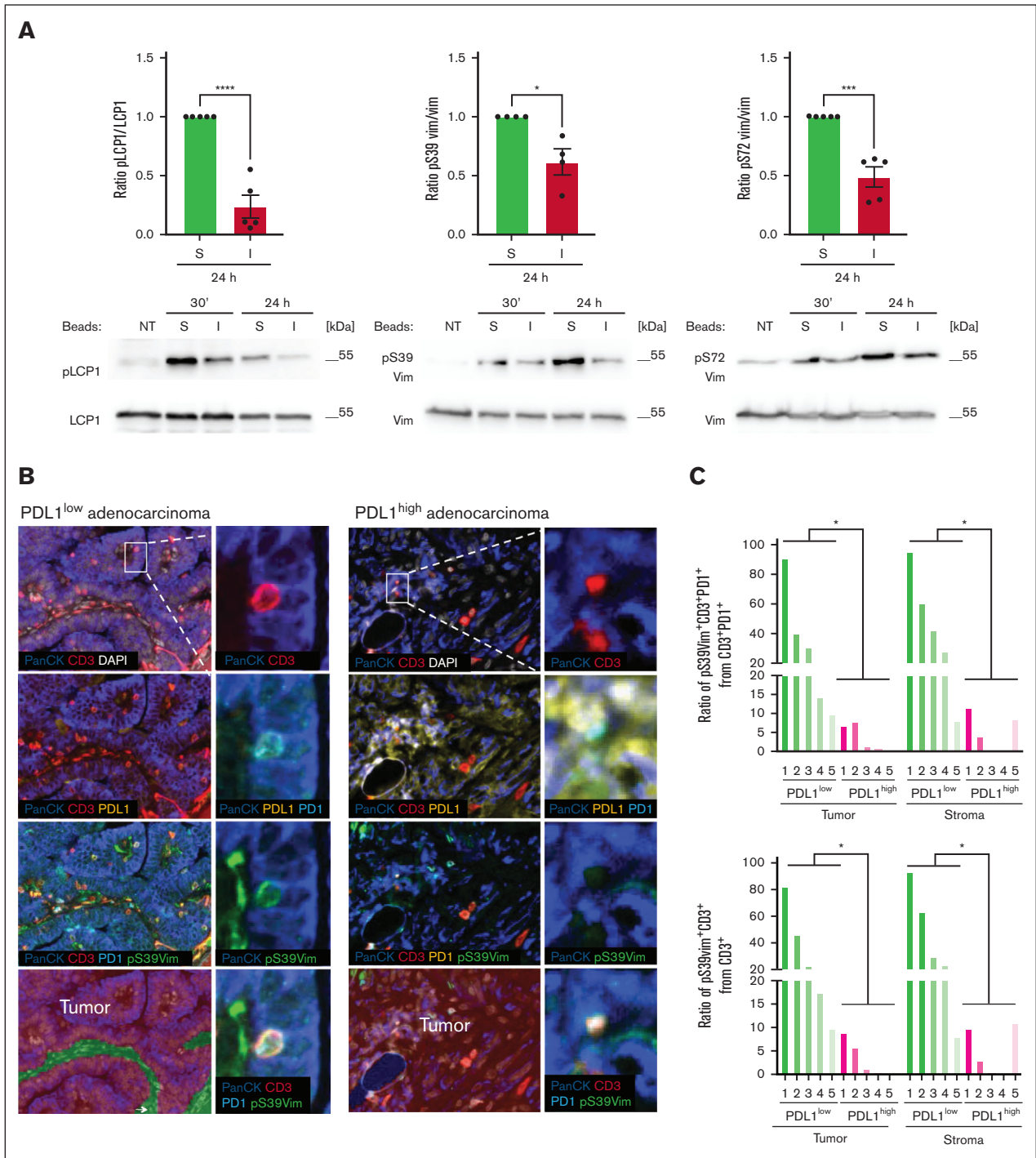


Figure 7. PD1 induces long-lasting dephosphorylation of cytoskeleton proteins in vitro and in human lung adenocarcinoma tissues. (A) Western blot analysis monitoring phosphorylation of S5 of L-plastin (pS5 LCP1), S39 of vimentin (pS39 Vim), and S72 of vimentin (pS72 Vim) in human primary CD4 T cells. Cells were left untreated (NT) or triggered for the indicated time points with stimulatory (S) or inhibitory (I) beads. Quantification of the signal at 24 hours was performed by normalization of the phosphorylation signal to the signal of nonphosphorylated total proteins and calculated for 4 (pS39 Vim) and 5 independent experiments (pS5 LCP1 and pS72 Vim). Mean value \pm SEM. Statistical analysis was performed using a 2-tailed, unpaired *t* test. **P* < .05; ****P* < .001; *****P* < .0001. (B) Immunohistochemistry staining of human lung adenocarcinoma tissue samples characterized by low or high PDL1 expression. Samples where fluorescently labeled for PanCK, PDL1, PD1, CD3 and pS39 Vim. Nuclei were visualized with DAPI. Insets show intratumoral CD3⁺ lymphocytes, positive for PD1, coexpressing pS39 Vim in the case of PDL1^{low} adenocarcinoma, and negative for pS39 Vim in PDL1^{high} adenocarcinoma. Images were acquired using Vectra Polaris imaging system. Images were segmented into “tumor” or “stroma” sections using the inForm software and based on PanCK and DAPI signals. (C) Quantification of the ratio of pS39Vim⁺ cells amongst CD3⁺PD1⁺ cells (left panel) or CD3⁺ cells (right panel) in tumor and stroma regions performed in 5 cases of PDL1^{low} and in 5 cases of PDL1^{high} human lung adenocarcinomas. Number of imaging fields collected per each case for PDL1^{low}: 1-21; 2-16; 3-19; case

both proteins colocalize in a molecular superstructure formed at the distal pole of regulatory T cells, opposite the IS, likely as a mechanism to augment the suppressive activity of regulatory T cells.³¹ Our data extend these findings by identifying vimentin as a PKC θ binding partner and PD1 target in the IS of effector T cells. Moreover, we identified the PKC θ -dependent vimentin phosphorylation sites S39 and S72 and provided proof-of-concept evidence for vimentin S39 phosphorylation as a biomarker indicating functional engagement of PD1 in tumor and stroma samples of patients with NSCLC. Although several lines of evidence support a correlation between PDL1 expression on tumors and response to therapy,⁵⁵⁻⁵⁷ not all PDL1 positive tumors respond to targeting the PD1/PDL1 axis. PDL1 expression can be induced through, tumor-intrinsic oncogenic pathways^{58,59}; it is not necessarily indicative of the intratumoral presence or fitness of T cells. Thus, a suitable marker predicting T-cell effector functions in combination with PDL1 expression might allow for better selection of patients who would benefit from therapeutic PD1/PDL1-targeting. Future studies should focus on measurement of vimentin S39 phosphorylation in PDL1⁺ tumors collected from responders and non-responders to PD1/PDL1-targeting therapies.

Our research lays the ground for future investigations into the role of PD1-induced cytoskeleton changes, which could yield precious mechanistic insight and identify further targets with therapeutic promise or utility as biomarkers for PD1-targeting immunotherapies.

Acknowledgments

The authors thank Nagham Alouche for assistance with flow cytometry-based experiments, Pascal Schneider for recombinant TACI-Fc, Giuseppe Pantaleo for providing the Jurkat-PD1 NFAT cell line, Marcus Long and Shiro Shibayama for valuable

discussions, advice, and critical review of the manuscript, Florence Morgenthaler for her assistance in confocal imaging, and Emilie Lingre for her help with multiplex immunofluorescence stainings.

L.d.L. and D.V. received funding from Swiss National Science Foundation grant 310030_172954. This study was supported by grants from Swiss Cancer Research (KFS-4095-02-2017-R; M.T.), the ISREC Foundation (S.P.), the Emma Muschamp foundation (M.T.), and a collaboration agreement with Ono Pharmaceutical (M.T.).

Authorship

Contribution: D.C. and M.T. developed the study concept, interpreted data, and prepared the manuscript; D.C., S.P., R.S., C.D., and M.G. performed experiments; M.T., D.C., and M.Q. designed the proteomic studies; M.Q. and D.C. performed and analyzed the proteomic studies; D.C. and K.B. designed the ImageStream experiments; K.B. performed and analyzed the ImageStream experiments; D.V., K.I., and L.d.L. designed the immunohistochemistry (IHC) experiments; D.V. and K.I. performed the IHC experiments; K.I., D.V., and L.d.L. analyzed the IHC experiments; and D.C. designed all other experiments, analyzed data, and prepared figures.

Conflict-of-interest disclosure: This study was supported by a collaboration agreement between M.T. and ONO Pharmaceutical, Japan. The remaining authors declare no competing financial interests.

ORCID profiles: S.P., 0009-0001-0704-5506; M.Q., 0000-0002-2720-4084; M.T., 0000-0002-5656-2139.

Correspondence: Margot Thome, Department of Immunobiology, University of Lausanne, Chemin des Boveresses 155, CH-1066, Epalinges, Switzerland; email: margot.thomemiazza@unil.ch.

References

- Courtney AH, Lo WL, Weiss A. TCR signaling: mechanisms of initiation and propagation. *Trends Biochem Sci*. 2018;43(2):108-123.
- Porciello N, Tuosto L. CD28 costimulatory signals in T lymphocyte activation: emerging functions beyond a qualitative and quantitative support to TCR signalling. *Cytokine Growth Factor Rev*. 2016;28:11-19.
- Thome M, Charton JE, Pelzer C, Hailfinger S. Antigen receptor signaling to NF-kappaB via CARMA1, BCL10, and MALT1. *Cold Spring Harb Perspect Biol*. 2010;2(9):a003004.
- Calvo V, Izquierdo M. Role of actin cytoskeleton reorganization in polarized secretory traffic at the immunological synapse. *Front Cell Dev Biol*. 2021;9:629097.
- Soares H, Lasserre R, Alcover A. Orchestrating cytoskeleton and intracellular vesicle traffic to build functional immunological synapses. *Immunol Rev*. 2013;256(1):118-132.
- Douanne T, Griffiths GM. Cytoskeletal control of the secretory immune synapse. *Curr Opin Cell Biol*. 2021;71:87-94.
- Beatty GL, Gladney WL. Immune escape mechanisms as a guide for cancer immunotherapy. *Clin Cancer Res*. 2015;21(4):687-692.
- Chamoto K, Yaguchi T, Tajima M, Honjo T. Insights from a 30-year journey: function, regulation and therapeutic modulation of PD1. *Nat Rev Immunol*. 2023;23(10):682-695.
- Arasanz H, Gato-Canas M, Zuazo M, et al. PD1 signal transduction pathways in T cells. *Oncotarget*. 2017;8(31):51936-51945.

Figure 7 (continued) 4-15; case 5-18. Number of imaging fields collected per each case for PDL1^{high}: 1-19; 2-22; 3-13; case 4-20; case 5-11. Number of tumor cells analysed per each case for PDL1^{low}: 1-30 853; 2-81 983; 3-60 988; 4-14 298; 5- 35 166. Number of tumor cells analysed per each case for PDL1^{high}: 1-5 900; 2-89 931; 3-27 363; 4-89 448; 5-20 981. Number of stroma cells analysed per each case for PDL1^{low}: 1-39 006; 2-31 193; 3-19 132; 4-32 378; 5-36 296. Number of stroma cells analysed per each case for PDL1^{high}: 1-112 832; 2-15 749; 3-10 887; 4-2; 5-51 525. Statistical analysis was performed using a 2-tailed, unpaired *t* test. **P* < .05.

10. Latchman Y, Wood CR, Chernova T, et al. PD-L2 is a second ligand for PD-1 and inhibits T cell activation. *Nat Immunol.* 2001;2(3):261-268.
11. Butte MJ, Keir ME, Phamduy TB, Sharpe AH, Freeman GJ. Programmed death-1 ligand 1 interacts specifically with the B7-1 costimulatory molecule to inhibit T cell responses. *Immunity.* 2007;27(1):111-122.
12. Messal N, Serriari NE, Pastor S, Nunes JA, Olive D. PD-L2 is expressed on activated human T cells and regulates their function. *Mol Immunol.* 2011;48(15-16):2214-2219.
13. Carlini MS, Larkin J, Long GV. Immune checkpoint inhibitors in melanoma. *Lancet.* 2021;398(10304):1002-1014.
14. Doroshow DB, Sanmamed MF, Hastings K, et al. Immunotherapy in non-small cell lung cancer: facts and hopes. *Clin Cancer Res.* 2019;25(15):4592-4602.
15. Massari F, Santoni M, Ciccarese C, et al. PD-1 blockade therapy in renal cell carcinoma: current studies and future promises. *Cancer Treat Rev.* 2015;41(2):114-121.
16. Xie W, Medeiros LJ, Li S, Yin CC, Khoury JD, Xu J. PD-1/PD-L1 pathway and its blockade in patients with classic Hodgkin lymphoma and non-Hodgkin large-cell lymphomas. *Curr Hematol Malig Rep.* 2020;15(4):372-381.
17. Das S, Johnson DB. Immune-related adverse events and anti-tumor efficacy of immune checkpoint inhibitors. *J Immunother Cancer.* 2019;7(1):306.
18. Chemnitz JM, Parry RV, Nichols KE, June CH, Riley JL. SHP-1 and SHP-2 associate with immunoreceptor tyrosine-based switch motif of programmed death 1 upon primary human T cell stimulation, but only receptor ligation prevents T cell activation. *J Immunol.* 2004;173(2):945-954.
19. Yokosuka T, Takamatsu M, Kobayashi-Imanishi W, Hashimoto-Tane A, Azuma M, Saito T. Programmed cell death 1 forms negative costimulatory microclusters that directly inhibit T cell receptor signaling by recruiting phosphatase SHP2. *J Exp Med.* 2012;209(6):1201-1217.
20. Celis-Gutierrez J, Blattmann P, Zhai Y, et al. Quantitative interactomics in primary T cells provides a rationale for concomitant PD-1 and BTLA coinhibitor blockade in cancer immunotherapy. *Cell Rep.* 2019;27(11):3315-3330.e7.
21. Hui E, Cheung J, Zhu J, et al. T cell costimulatory receptor CD28 is a primary target for PD-1-mediated inhibition. *Science.* 2017;355(6332):1428-1433.
22. Okazaki T, Maeda A, Nishimura H, Kurosaki T, Honjo T. PD-1 immunoreceptor inhibits B cell receptor-mediated signaling by recruiting src homology 2-domain-containing tyrosine phosphatase 2 to phosphotyrosine. *Proc Natl Acad Sci U S A.* 2001;98(24):13866-13871.
23. Patsoukis N, Duke-Cohan JS, Chaudhri A, et al. Interaction of SHP-2 SH2 domains with PD-1 ITSM induces PD-1 dimerization and SHP-2 activation. *Commun Biol.* 2020;3(1):128.
24. Sheppard KA, Fitz LJ, Lee JM, et al. PD-1 inhibits T-cell receptor induced phosphorylation of the ZAP70/CD3zeta signalosome and downstream signaling to PKCtheta. *FEBS Lett.* 2004;574(1-3):37-41.
25. Navarro MN, Cantrell DA. Serine-threonine kinases in TCR signaling. *Nat Immunol.* 2014;15(9):808-814.
26. Neal JW, Clipstone NA. Calcineurin mediates the calcium-dependent inhibition of adipocyte differentiation in 3T3-L1 cells. *J Biol Chem.* 2002;277(51):49776-49781.
27. Hallal M, Braga-Lagache S, Jankovic J, et al. Inference of kinase-signaling networks in human myeloid cell line models by Phosphoproteomics using kinase activity enrichment analysis (KAEA). *BMC Cancer.* 2021;21(1):789.
28. Cox J, Mann M. MaxQuant enables high peptide identification rates, individualized p.p.b.-range mass accuracies and proteome-wide protein quantification. *Nat Biotechnol.* 2008;26(12):1367-1372.
29. Keller A, Nesvizhskii AI, Kolker E, Aebersold R. Empirical statistical model to estimate the accuracy of peptide identifications made by MS/MS and database search. *Anal Chem.* 2002;74(20):5383-5392.
30. Patsoukis N, Bardhan K, Chatterjee P, et al. PD-1 alters T-cell metabolic reprogramming by inhibiting glycolysis and promoting lipolysis and fatty acid oxidation. *Nat Commun.* 2015;6:6692.
31. McDonald-Hyman C, Muller JT, Loschi M, et al. The vimentin intermediate filament network restrains regulatory T cell suppression of graft-versus-host disease. *J Clin Invest.* 2018;128(10):4604-4621.
32. Riplinger SM, Wabnitz GH, Kirchgessner H, et al. Metastasis of prostate cancer and melanoma cells in a preclinical in vivo mouse model is enhanced by L-plastin expression and phosphorylation. *Mol Cancer.* 2014;13:10.
33. Wang C, Morley SC, Donermeyer D, et al. Actin-bundling protein L-plastin regulates T cell activation. *J Immunol.* 2010;185(12):7487-7497.
34. Wabnitz GH, Kocher T, Lohneis P, et al. Costimulation induced phosphorylation of L-plastin facilitates surface transport of the T cell activation molecules CD69 and CD25. *Eur J Immunol.* 2007;37(3):649-662.
35. Hivroz C, Saitakis M. Biophysical aspects of T lymphocyte activation at the immune synapse. *Front Immunol.* 2016;7:46.
36. Rueda D, Gaide O, Ho L, et al. Bcl10 controls TCR- and FcgammaR-induced actin polymerization. *J Immunol.* 2007;178(7):4373-4384.
37. Rota G, Niogret C, Dang AT, et al. Shp-2 is dispensable for establishing T cell exhaustion and for PD-1 signaling in vivo. *Cell Rep.* 2018;23(1):39-49.
38. Ventura PMO, Gakovic M, Fischer BA, et al. Concomitant deletion of Ptpn6 and Ptpn11 in T cells fails to improve anticancer responses. *EMBO Rep.* 2022;23(11):e55399.
39. Xu X, Hou B, Fulzele A, et al. PD-1 and BTLA regulate T cell signaling differentially and only partially through SHP1 and SHP2. *J Cell Biol.* 2020;219(6):e201905085.
40. Zhang T, Guo W, Yang Y, et al. Loss of SHP-2 activity in CD4+ T cells promotes melanoma progression and metastasis. *Sci Rep.* 2013;3:2845.

41. Li Z, McNulty DE, Marler KJ, et al. IQGAP1 promotes neurite outgrowth in a phosphorylation-dependent manner. *J Biol Chem*. 2005;280(14):13871-13878.
42. Ratnayake WS, Apostolatos CA, Apostolatos AH, et al. Oncogenic PKC- γ activates vimentin during epithelial-mesenchymal transition in melanoma; a study based on PKC- γ and PKC- ζ specific inhibitors. *Cell Adh Migr*. 2018;12(5):447-463.
43. Sasahara Y, Rachid R, Byrne MJ, et al. Mechanism of recruitment of WASP to the immunological synapse and of its activation following TCR ligation. *Mol Cell*. 2002;10(6):1269-1281.
44. Liu Y, Graham C, Li A, Fisher RJ, Shaw S. Phosphorylation of the protein kinase C-theta activation loop and hydrophobic motif regulates its kinase activity, but only activation loop phosphorylation is critical to in vivo nuclear-factor-kappaB induction. *Biochem J*. 2002;361(Pt 2):255-265.
45. Monks CR, Kupfer H, Tamir I, Barlow A, Kupfer A. Selective modulation of protein kinase C-theta during T-cell activation. *Nature*. 1997;385(6611):83-86.
46. Liu Y, Witte S, Liu YC, Doyle M, Elly C, Altman A. Regulation of protein kinase C theta function during T cell activation by Lck-mediated tyrosine phosphorylation. *J Biol Chem*. 2000;275(5):3603-3609.
47. Bi K, Tanaka Y, Coudronniere N, et al. Antigen-induced translocation of PKC-theta to membrane rafts is required for T cell activation. *Nat Immunol*. 2001;2(6):556-563.
48. Mielgo-Rubio X, Uribealarea EA, Cortés LQ, Moyano MS. Immunotherapy in non-small cell lung cancer: update and new insights. *J Clin Transl Res*. 2021;7(1):1-21.
49. Ruiz-Cordero R, Devine WP. Targeted therapy and checkpoint immunotherapy in lung cancer. *Surg Pathol Clin*. 2020;13(1):17-33.
50. Esensten JH, Helou YA, Chopra G, Weiss A, Bluestone JA. CD28 costimulation: from mechanism to therapy. *Immunity*. 2016;44(5):973-988.
51. Duraiswamy J, Turrini R, Minasyan A, et al. Myeloid antigen-presenting cell niches sustain antitumor T cells and license PD-1 blockade via CD28 costimulation. *Cancer Cell*. 2021;39(12):1623-1642.e20.
52. Kamphorst AO, Wieland A, Nasti T, et al. Rescue of exhausted CD8 T cells by PD-1-targeted therapies is CD28-dependent. *Science*. 2017;355(6332):1423-1427.
53. Tocheva AS, Peled M, Strazza M, et al. Quantitative phosphoproteomic analysis reveals involvement of PD-1 in multiple T cell functions. *J Biol Chem*. 2020;295(52):18036-18050.
54. Paillon N, Mouro V, Dogniaux S, et al. PD-1 inhibits T cell actin remodeling at the immunological synapse independently of its signaling motifs. *Sci Signal*. 2023;16(813):eadh2456.
55. Aguilar EJ, Ricciuti B, Gainor JF, et al. Outcomes to first-line pembrolizumab in patients with non-small-cell lung cancer and very high PD-L1 expression. *Ann Oncol*. 2019;30(10):1653-1659.
56. Reck M, Rodríguez-Abreu D, Robinson AG, et al. Pembrolizumab versus chemotherapy for PD-L1-positive non-small-cell lung cancer. *N Engl J Med*. 2016;375(19):1823-1833.
57. Taube JM, Klein A, Brahmer JR, et al. Association of PD-1, PD-1 ligands, and other features of the tumor immune microenvironment with response to anti-PD-1 therapy. *Clin Cancer Res*. 2014;20(19):5064-5074.
58. Jiang X, Zhou J, Giobbie-Hurder A, Wargo J, Hodi FS. The activation of MAPK in melanoma cells resistant to BRAF inhibition promotes PD-L1 expression that is reversible by MEK and PI3K inhibition. *Clin Cancer Res*. 2013;19(3):598-609.
59. Marzec M, Zhang Q, Goradia A, et al. Oncogenic kinase NPM/ALK induces through STAT3 expression of immunosuppressive protein CD274 (PD-L1, B7-H1). *Proc Natl Acad Sci U S A*. 2008;105(52):20852-20857.